Shape Optimization of Unstructured Lattices

Antonin Paquette-Rufiange[1], Serge Prudhomme[1], and Marc Laforest[1]

[1] *Département de mathématiques et de génie industriel, École Polytechnique de Montréal, Montréal, Québec, Canada, H3T 1J4*

September 25, 2018

Abstract

This paper presents a methodology for optimizing the shape of unstructured lattices produced by additive manufacturing technologies. The lattices are modeled as a collection of one-dimensional beams under external loadings. The formulations of the shape optimization problems, which aim at minimizing the strain energy of the lattices when subjected to geometrical constraints, are described in detail. The work mainly focuses on the theoretical and numerical analysis of these formulations. The performance of the proposed method is also assessed on several test cases.

Keywords: Shape Optimization, Lattices, Unstructured Meshes, Additive Manufacturing, Non-Linear Constrained Problem

1 Introduction

Fabrication of lattice structures by rapidly evolving additive manufacturing technologies now allows one to contemplate innovative designs for mechanical parts such as lattice structures whose main advantage are to presserve the mechanical properties of solid parts while being lightweight. Lattices structures are actually drawing the attention of several industrial sectors, in particular in aeronautics and biomechanics. For example, medical prostheses composed of lattices present enhanced biocompatibility and can be personalized to the patients needs [13, 24]. Lattice structures embedded in planes or cars can help reduce their overall mass and lead to significant reduction in fuel consumption [11].

In order to fully take advantage of the extensive freedom of design offered by additive manufacturing technologies, several optimization techniques have been developed over the past years. One of the well-known methods in topology optimization is the Solid Isotropic Material Penalization (SIMP) [2, 3, 20], which consists in subdivising a geometry into cells and fills with material those which are relevant to a particular functionnal objective. Due to the high geometrical complexity of the parts designed with the SIMP method, several works have attempted to directly bridge the method with additive manufacturing technologies. Some have considered, for example, to fill intermediate density regions with predefined lattice cells [4, 18]. The process relies however on heuristics regarding the choice and the size of the cells.

Another topology optimization technique is the **Ground Structure Method (GSM), also known as Layout Optimization** [1, 9, 21, 25]. This method consists in optimizing the cross-section area of trusses connecting a dense set of points inside a domain. Extensions of the method have been developed to seek the optimal position of the nodes and to consider the buckling phenomenon in the optimization problem [7, 26]. To the best of the authors' knowledge, this topology optimization method only considers the trusses as bars, hence only taking into account the axial forces and deformations.

The authors in [5] followed the idea of finding the optimal position of the nodes inside a given lattice. They considered a set of trusses linked by nodes inside a geometry and sought the position of these nodes and the size of the trusses such that the compliance is minimized. They conducted experiments on printed parts and observed that the optimized structures possessed enhanced mechanical properties compared to non-optimized parts.

The objectives of the paper are to present and describe a methodology to optimize the shape of unstructured lattices. The proposed method resembles the approach taken in [5]. A simple geometrical and mechanical description of an unstructured lattice leads to consistent definitions of objective and constraint functions **unlike the SIMP or GSM formulations**. These definitions are then used to formulate two shape optimization problems. The principal contribution addressed in this work is the analysis of the shape optimization problems, in particular whether or not there exist solutions to the shape optimization problems depending of the type of constraints. We evaluate analytically and numerically the impact of the added constraints for various problems. Finally, we address the question as to whether the creation of unstructured lattices is advantageous compared to their structured counterpart.

The paper is organized as follows. We present in Section 2 the geometrical description of a lattice structure and introduce the hypotheses employed in order to model the structure. In Section 3, we present the mechanical model of a lattice. In Section 4, we first formulate the different shape optimization problems to be studied. We then propose strategies designed to efficiently solve the various shape optimization problems. We briefly present the interior-point method to solve finite-dimensional optimization problem with equality and inequality constraints. The reduced and adjoint problems are also described in order to efficiently compute the **gradient** of the objective function. In Section 5, we apply the different shape optimization problems on several numerical examples. We first discuss the well-posedness of these problems using some simple examples. We then solve the shape optimization problem on denser lattices with more complex loadings. We finally conclude and discuss the performance of the proposed methodology in Section 6.

2 Geometrical Model

In this section, we first present the geometrical characteristics of the lattice and lay out some hypotheses underlying a lattice model. Let Ω denote a polyhedral open subset of $\mathbb{R}^d$, $d \in \{2, 3\}$, representing the region occupied by a solid that should be replaced by a lattice structure. We assume that the boundary of Ω, denoted by $\partial\Omega$, is formed of N_Γ $(d-1)$-simplices noted Γ_k, $k = 1, \dots, N_\Gamma$. For the sake of clarity, we will no distinguish a simplex from the subset generated by the convex combination of the element of the simplex. Following [6, Chapter 2], we define a triangulation/mesh $\mathcal{T}_h$ of the closure of Ω by partitioning the closure of Ω into a set K of N_k d-simplices. These d-simplices will be referred to as elements (an usual designation in the finite element literature). Consistency of the mesh $\mathcal{T}_h$ requires that the intersection of two distinct elements $K_e, K_f \in K$ that possess a non-trivial intersection $K_e \cap K_f \neq \varnothing$ must forms a k-simplex with $k \leq d - 1$. We recall that a d-simplex is a point for $d = 0$, a segment for $d = 1$, a triangle for $d = 2$, and a tetrahedron for $d = 3$. The triangulation/mesh $\mathcal{T}_h$ provides also a connectivity $\mathcal{M}$ that specifies the connection between all simplices of $\mathcal{T}$.

Definition 1 (Lattice) *Every 0-simplex of the mesh $\mathcal{T}_h$ serves as support for a point of null measure. The set of the N_P points is denoted by P. Every 1-simplex (edge) of the mesh $\mathcal{T}_h$ serve as support for a three dimensional cylindrical truss whose axis coincide with its associated 1-simplices. The set of N_T cylindrical trusses is noted T. A lattice L is the union of the set P of all the point and the set T of all trusses. By neglecting the overlaps of the trusses at the vicinity of a point (Figure 3), the volume vol of the lattice L is the sum of the volume of the trusses.*

This definition of a lattice L allows the inheritance of the notion of elements K_e and connectivity $\mathcal{M}$. For the sake of clarity, we will now refer to K as the set of elements K_e that are circumvented by the axis of the trusses T_m and to $\mathcal{M}$ as the connectivity of the points $x_i \in P$. We can **breakdown** the set P of all points into more specific sets. We denote by P_I the set of points that belong to Ω ($P_I = \{x_i \in P \,|\, x_i \in \Omega\}$). We note by P_{Γ_i} the set of points that belong to the boundary Γ_i ($P_{\Gamma_i} = \{x_i \in P \,|\, x_i \in \Gamma_i\}$). The procedure of creation of a lattice is presented in Figure 1 on an L-shaped domain Ω.

The final objective is to manufacture any lattice satisfying the engineering objectives, but the manufacturing process already brings with it two simple constraints.

Manufacturing Constraints 1 *Each element K_e should be large enough that its trusses can be manufactured as a separate piece.*

Manufacturing Constraints 2 *Trusses should be either parallel to the printing plane, or angled above Θ_p with respect to that plane.*

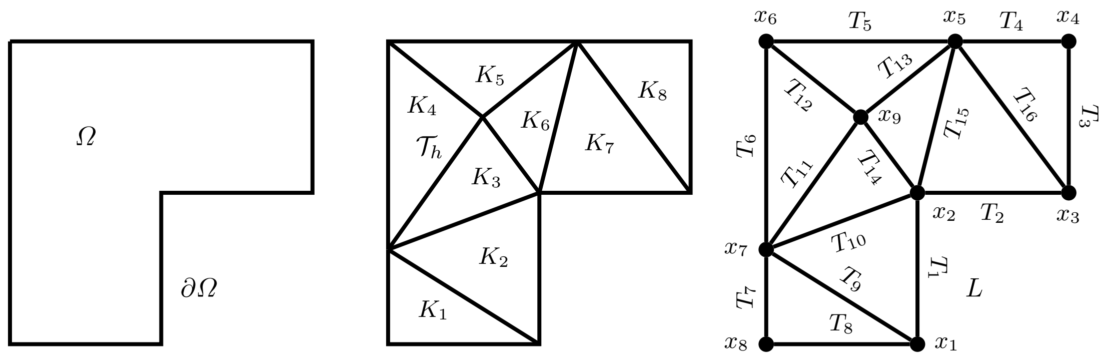

Figure 1: (Left) Illustration of a polygonal domain $\Omega \in \mathbb{R}^2$ of a solid to be replaced by a lattice. (Center) Mesh $\mathcal{T}_h$ of domain Ω. (Right) Illustration of lattice L extracted from $\mathcal{T}_h$.

The constraint 2 will be briefly discussed in Section 4, but we remark that this constraints has variables importance depending of the additive manufacturing technique. The constraint 1 requires that the trusses be of a minimum length and that the angles between trusses also remain above a minimum angle, both determined by the manufacturing process. This constraint is therefore equivalent to a constraint on the uniformity of the elements K_e of the mesh $\mathcal{T}_h$.

The choice of a triangular/tetrahedral mesh instead of an arbitrary polygonal/polyhedral mesh is justified by the widely and extensive literature dealing with triangular/tetrahedral mesh generation, adaptation, and quality. One can have considered **quadrangle** mesh, but we suppose that a nearly equilateral triangular elements distribute more uniformly forces under multiples loadings. We now introduce a particular mesh quality measure for guiding the shape optimization process, in order to produce meshes that favor equilateral triangles. The reader is referred to [17] for a thorough presentation and comparison of several quality measures.

The quality measure employed in this work is related to the condition number of the mapping from a reference element to an actual element [8, 12]. For the sake of clarity, we present the quality measure for triangular elements. The same procedure can be applied to tetrahedral elements. Let K_e be an arbitrary element of lattice L. The affine mapping is denoted by M_{K_e} and maps an equilateral reference element $\hat{K}$ to the real element K_e (see Figure 2).

Let $\{x_1, x_2, x_3\}$ (with $x_i = (x_{x,i}, x_{y,i}) \in \mathbb{R}^2$) be the vertices of element K_e. The affine mapping from $\hat{K}$ to K_e is given by

$$\boldsymbol{x} = M_{K_e}(\boldsymbol{\xi}) = \underbrace{\begin{bmatrix} x_{x,2} - x_{x,1} & \frac{1}{\sqrt{3}}\left(x_{x,3} - x_{x,1} + x_{x,3} - x_{x,2}\right) \\ x_{y,2} - x_{y,1} & \frac{1}{\sqrt{3}}\left(x_{y,3} - x_{y,1} + x_{y,3} - x_{y,2}\right) \end{bmatrix}}_{G_{K_e}} \boldsymbol{\xi} + \begin{bmatrix} x_{x,1} \\ x_{y,1} \end{bmatrix}. \tag{2.1}$$

The condition number of matrix G_{K_e} with respect to the Frobenius norm $\|A\|_F := \sqrt{\sum_i \sum_j A_{ij}^2}$ is

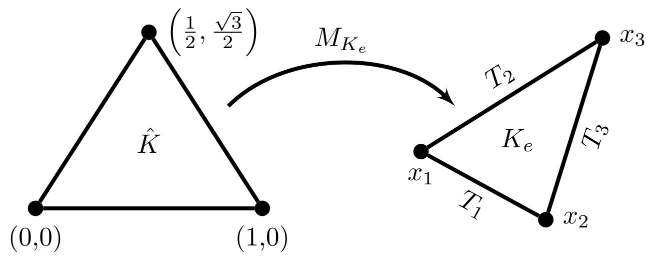

Figure 2: Affine mapping M_{K_e} from the equilateral reference element $\hat{K}$ to an element K_e.

given by

$$\kappa(K_e) = \|G_{K_e}\|_F \|G_{K_e}^{-1}\|_F. \tag{2.2}$$

Note that G_K is actually the Jacobian matrix of M_K. The choice of the Frobenius norm is motivated by the fact that it is differentiable with respect to the position of the nodes x_i while other norms like $\|\cdot\|_1$ or $\|\cdot\|_\infty$ are not. One could have instead chosen the induced norm $\|\cdot\|_2$ but it was shown in [17] that the corresponding condition numbers are essentially the same as those computed from the Frobenius norm. One can show that for each element $K_e \in K$, $\kappa(K_e) \geq 2$, $\forall K$, hence the normalized quality measure we propose is

$$c_\kappa(K_e) := \frac{2}{\kappa(K_e)}. \tag{2.3}$$

This quality measure indicates whether element K_e is an equilateral triangle ($c_\kappa(K_e) = 1$) or close to a degenerated triangle ($c_\kappa(K_e) \to 0$) [17]. It is important to note that the quality measure is invariant under translation, rotation, and scaling of the elements.

3 Mechanical Model

The objective of this section is to derive a mathematical model of a lattice subjected to external traction forces. The model should be simple enough so that the optimization problem be tractable, yet accurate enough to describe the correct mechanical behavior of the lattice. We shall suppose here that the lattice is made of a linear elastic isotropic material and thus neglect the material orthotropicity due to the manufacturing process. The mechanical properties are then fully described by the Young modulus E and Poisson ratio ν of the material. We will assume that homogeneous Dirichlet boundary conditions are prescribed on part of the lattice boundary, denoted by ∂L_u, and that tractions $t = (t_x, t_y, t_z)$ are applied to the remainder of the lattice boundary, denoted by ∂L_t. The total energy in the lattice, as a function of the displacement field $u = (u_x, u_y, u_z)$, is then given by:

$$\mathcal{J}(u) = \mathcal{E}(u) - \mathcal{W}(u), \tag{3.1}$$

where $\mathcal{E}(u)$ and $\mathcal{W}(u)$ are the strain energy and external energy, respectively,

$$\mathcal{E}(u) = \frac{1}{2}\int_L C_{ijkl}\epsilon_{kl}(u)\epsilon_{ij}(u)\, d,x \tag{3.2}$$

$$\mathcal{W}(u) = \int_{\partial L_t} t_i u_i \, ds. \tag{3.3}$$

Here, $C = C(E, \nu)$ is the fourth-order stiffness tensor defined in terms of E and ν and $\epsilon_{ij}(u)$ denotes the second-order strain tensor:

$$\epsilon_{ij}(u) = \frac{1}{2}\left(\frac{\partial u_i}{\partial x_j} + \frac{\partial u_j}{\partial x_i}\right). \tag{3.4}$$

The second-order stress tensor is denoted by:

$$\sigma_{ij} = C_{ijkl}\epsilon_{lk}. \tag{3.5}$$

Note that the Einstein convention on repeated indices is used throughout the paper.

Let $V = \{u \in [H^1(L)]^3 \,|\, u = 0 \text{ on } \partial L_u\}$ denote the spaces of admissible solutions and test functions. The displacement field $u \in V$ in the lattice at equilibrium is thus given by

$$u = \underset{v\in V}{\operatorname{argmin}}\, \mathcal{J}(v). \tag{3.6}$$

Above minimization problem is obviously equivalent to the variational problem:

$$\text{Find } u \in V \text{ such that:} \qquad \int_L C_{ijkl}\epsilon_{kl}(u)\epsilon_{ij}(v)\, dx = \int_{\partial L_t} t_i v_i \, ds, \qquad \forall v \in V. \tag{3.7}$$

The three-dimensional variational problem is clearly computationally intractable if the lattice is made of a very large number of trusses. Our objective is thus to construct a reduced model in order to decrease the number of degrees of freedom in the system. The approach that we shall follow is to model each truss of the lattice using unidimensional bar or Euler-Bernoulli models. With the definition of a lattice (Definition 1), the problem (3.7) can be reformulated as follows:

$$\text{Find } u \in V \text{ such that:} \qquad \sum_{m=1}^{N_T}\left[\int_{T_m} C_{ijkl}\epsilon_{kl}(u)\epsilon_{ij}(v)\, dx - \int_{T_m\cap\partial L_t} t_i v_i \, ds\right] = 0, \qquad \forall v \in V. \tag{3.8}$$

The objective is to consider local problems on each truss and to recover Problem (3.8) by enforcing the continuity of the displacement field and ensuring the balance of the forces and moments at the nodes of the lattice. We describe the unidimensional problem on a reference truss in the next section and later derive the global reduced model.

3.1 1D model of truss in a reference system

The following presentation is partially inspired by [16]. We consider here a reference truss $\hat{T}$ of length ℓ and constant cross-sectional area A in the local coordinate system $(\mathcal{O}, \xi, \eta, \zeta)$, see Figure 4.

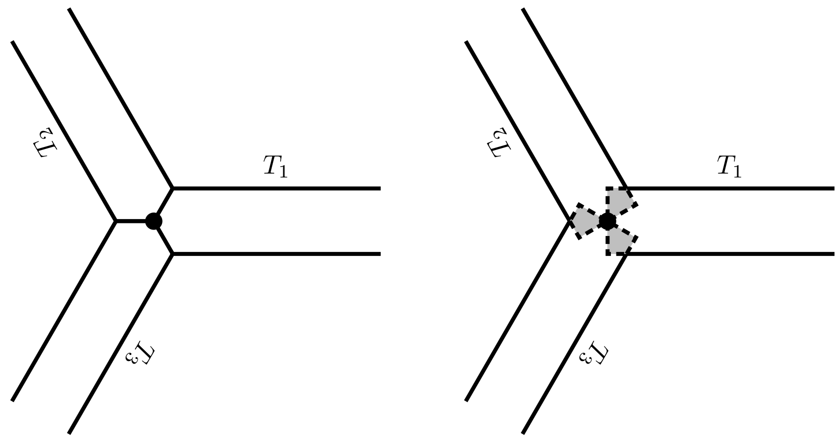

Figure 3: (Left) Junction of trusses T_1, T_2, and T_3 for a manufactured lattice. (Right) Overlaps of trusses T_1, T_2, and T_3 for the lattice L.

We denote by $\hat{x}_0$ and $\hat{x}_1$ the nodes at the extremities of the truss with coordinates $(0, 0, 0)$ and $(\ell, 0, 0)$, respectively.

The Euler-Bernoulli model states that the displacement field of a truss aligned in the ξ-direction is given by:

$$u(\xi) = \begin{bmatrix} f(\xi) - \eta \dfrac{dg}{d\xi}(\xi) \\ g(\xi) \\ 0 \end{bmatrix} \tag{3.9}$$

where f and g are functions of the independent variable ξ only. Again, for the sake of clarity, we present the Euler-Bernoulli model for displacements and deformations in the $\xi\eta$-plane, but the description can easily be extended to a 3D framework. The function f describes the displacement due to compression and tension forces. The quantity $\theta = dg/d\xi$ defines the angle of rotation of the cross-sections with respect to the ζ-axis, due to normal forces and moments. We note that the Euler-Bernoulli model assumes that the cross-sections of the truss remain perpendicular to the neutral axis of the truss, as illustrated in Figure 4.

In the Euler-Bernoulli model, the torsion effects are neglected. We also note that we recover the so-called bar model by taking $g(\xi) = 0$, in which case $\theta(\xi) = 0$, $\forall \xi \in [0, \ell]$. We believe that the Euler-Bernoulli model, which takes into account axial as well as bending stresses, should provide an accurate description of the mechanical behavior of the trusses in a lattice. If the model is in fact invalidated, one could consider more complex models, such as the Timoshenko model, non-linear models, or even a full finite element model of the truss. Validation of the Euler-Bernoulli for lattices will be the subject of a future study.

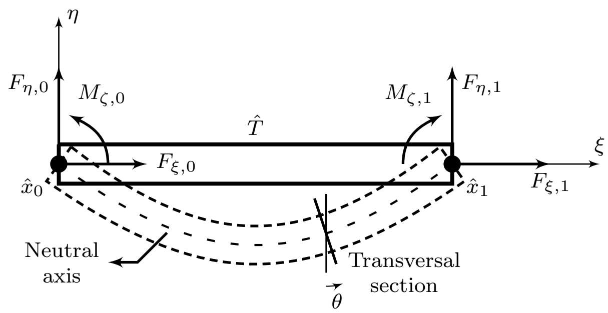

Figure 4: Forces $F_{\eta,0}$ and $F_{\eta,1}$ and moments $M_{\zeta,0}$ and $M_{\zeta,1}$ applied to a reference truss $\hat{T}$ using the Euler-Bernoulli model.

Using (3.9), the strain $\epsilon_{\hat{T}}$ in truss $\hat{T}$ is given by:

$$\epsilon_{\hat{T}}(u) = \begin{bmatrix} \dfrac{df}{d\xi} - \eta \dfrac{d^2 g}{d\xi^2} & 0 & 0 \\ 0 & 0 & 0 \\ 0 & 0 & 0 \end{bmatrix} \tag{3.10}$$

Ignoring the Poisson effects in the beam (setting $\nu = 0$), the stress tensor $\sigma_{\hat{T}}$ in truss $\hat{T}$ is calculated as:

$$\sigma_{\hat{T}}(u) = \begin{bmatrix} E\dfrac{df}{d\xi} - E\eta \dfrac{d^2 g}{d\xi^2} & 0 & 0 \\ 0 & 0 & 0 \\ 0 & 0 & 0 \end{bmatrix} \tag{3.11}$$

where E is the Young's modulus of the truss. It is important to note that since we consider the material to be isotropic, the definition of the stiffness tensor C is the same for the reference truss $\hat{T}$ than that for an arbitrary truss T_m. It follows that the strain energy $\mathcal{E}_{\hat{T}}$ reads:

$$\mathcal{E}_{\hat{T}}(u) = \frac{1}{2}\int_{\hat{T}} C_{ijkl}\epsilon_{kl}(u)\epsilon_{ij}(u)\, d\xi d\eta d\zeta = \frac{1}{2}\int_{\hat{T}} \sigma_{11}(u)\epsilon_{11}(u)\, d\xi d\eta d\zeta \tag{3.12}$$

which can be rewritten with respect to the functions (f, g) as:

$$\mathcal{E}_{\hat{T}}(f, g) = \frac{1}{2}\int_0^{\ell} \left[EA\left(\frac{df}{d\xi}\right)^2 + EI_\zeta \left(\frac{d^2 g}{d\xi^2}\right)^2 \right] d\xi. \tag{3.13}$$

where I_ζ is the moment of inertia with respect to the ζ-axis. The idea is now to calculate the forces and moments at the boundaries of truss $\hat{T}$, when the endpoints are subjected to prescribed displacements and angles of rotation. In order to set the minimization problems, we first introduce the following spaces of functions:

$$
\begin{aligned}
X &= \{f \in H^1(0,\ell) :\ f(0) = f_0,\ f(\ell) = f_1\},\\
X_0 &= \{f \in H^1(0,\ell) :\ f(0) = 0,\ f(\ell) = 0\},\\
Y &= \{g \in H^2(0,\ell) :\ g(0) = g_0,\ g(\ell) = g_1,\ g'(0) = \theta_0,\ g'(\ell) = \theta_1\},\\
Y_0 &= \{g \in H^2(0,\ell) :\ g(0) = 0,\ g(\ell) = 0,\ g'(0) = 0,\ g'(\ell) = 0\},
\end{aligned}
$$

where $\{f_0, f_1\}$, and $\{g_0, g_1, \theta_0, \theta_1\}$ are the prescribed boundary values. The minimization problem is thus:

$$
(f, g) = \underset{(\hat{f},\hat{g})\in X\times Y}{\operatorname{argmin}}\ \mathcal{E}_{\hat{T}}(\hat{f}, \hat{g}). \tag{3.14}
$$

Equivalently, above problem leads to the system of decoupled variational problems:

$$
\text{Find } f \in X \text{ such that:} \qquad \int_0^\ell EA\frac{df}{d\xi}\frac{dp}{d\xi}d\xi = 0, \qquad \forall p \in X_0, \tag{3.15}
$$

$$
\text{Find } g \in Y \text{ such that:} \qquad \int_0^\ell EI_\zeta\frac{d^2g}{d\xi^2}\frac{d^2q}{d\xi^2}d\xi = 0, \qquad \forall q \in Y_0. \tag{3.16}
$$

These problems can be recast in strong form as:

$$
\frac{d}{d\xi}\left(EA\frac{df}{d\xi}\right) = 0, \quad \forall \xi \in (0,\ell), \quad \text{with } f(0) = f_0,\ f(\ell) = f_1, \tag{3.17}
$$

$$
\frac{d^2}{d\xi^2}\left(EI_\zeta\frac{d^2g}{d\xi^2}\right) = 0, \quad \forall \xi \in (0,\ell), \quad \text{with } g(0) = g_0,\ \frac{dg}{d\xi}(0) = \theta_0,\ g(\ell) = g_1,\ \frac{dg}{d\xi}(\ell) = \theta_1. \tag{3.18}
$$

In the case where the parameters E, A, and I_ζ remain constant along the truss, the analytical solutions of these problems are simply given by:

$$
f(\xi) = f_0\left(1 - \frac{\xi}{\ell}\right) + f_1\frac{\xi}{\ell}, \tag{3.19a}
$$

$$
g(\xi) = \theta_0\xi\left(1 - \frac{\xi}{\ell}\right)^2 - \theta_1\frac{\xi^2}{\ell^2}(\ell - \xi) - g_0\left(1 - \frac{\xi}{\ell}\right)\left(2\frac{\xi^2}{\ell^2} - 1\right) + g_1\frac{\xi^2}{\ell^2}\left(3 - 2\frac{\xi}{\ell}\right). \tag{3.19b}
$$

The axial forces at the nodes $\hat{x}_0$ and $\hat{x}_1$ are denoted by $F_{\xi,0}$ and by $F_{\xi,1}$ respectively, while the tangential forces are denoted by $F_{\eta,0}$ and $F_{\eta,1}$ (see Figure 4). These four forces are given by:

$$
F_{\xi,0} = -EA\frac{df}{d\xi}(0) = \frac{EA}{\ell}\left(f_0 - f_1\right), \tag{3.20a}
$$

$$
F_{\xi,1} = EA\frac{df}{d\xi}(\ell) = -\frac{EA}{\ell}\left(f_0 - f_1\right), \tag{3.20b}
$$

$$
F_{\eta,0} = \frac{d}{d\xi}\left(EI_\zeta\frac{d^2g}{d\xi^2}\right)(0) = 6\frac{EI_\zeta}{\ell^3}\left(2g_0 + \ell\theta_0 - 2g_1 + \ell\theta_1\right), \tag{3.20c}
$$

$$
F_{\eta,1} = -\frac{d}{d\xi}\left(EI_\zeta\frac{d^2g}{d\xi^2}\right)(\ell) = -6\frac{EI_\zeta}{\ell^3}\left(2g_0 + \ell\theta_0 - 2g_1 + \ell\theta_1\right). \tag{3.20d}
$$

On the other hand, the moments $M_{\zeta,0}$ and $M_{\zeta,1}$ at the nodes $\hat{x}_0$ and $\hat{x}_1$ are computed as:

$$M_{\zeta,0} = -EI_\zeta \frac{d^2 g}{d\xi^2}(0) = \frac{EI_\zeta}{\ell^2}\left(6g_0 - 6g_1 + 4\ell\theta_0 + 2\ell\theta_1\right), \tag{3.21a}$$

$$M_{\zeta,1} = \quad EI_\zeta \frac{d^2 g}{d\xi^2}(\ell) = \frac{EI_\zeta}{\ell^2}\left(6g_0 - 6g_1 + 2\ell\theta_0 + 4\ell\theta_1\right). \tag{3.21b}$$

The forces and moments have now been evaluated at the endpoints of the truss in terms of the input parameters $\{f_0, f_1\}$ and $\{g_0, g_1, \theta_0, \theta_1\}$, i.e. the displacements and angles of rotation at $\xi = 0$ and $\xi = \ell$. Since the equations (3.20) and (3.21) are linear with respect to $\{f_0, f_1\}$ and $\{g_0, g_1, \theta_0, \theta_1\}$, one can represent these equations in matrix form:

$$\underbrace{\begin{bmatrix} EA\ell^{-1} & 0 & 0 & -EA\ell^{-1} & 0 & 0 \\ 0 & 12EI_\zeta\ell^{-3} & 6EI_\zeta\ell^{-2} & 0 & -12EI_\zeta\ell^{-3} & 6EI_\zeta\ell^{-2} \\ 0 & 6EI_\zeta\ell^{-2} & 4EI_\zeta\ell^{-1} & 0 & -6EI_\zeta\ell^{-2} & 2EI_\zeta\ell^{-1} \\ -EA\ell^{-1} & 0 & 0 & EA\ell^{-1} & 0 & 0 \\ 0 & -12EI_\zeta\ell^{-3} & -6EI_\zeta\ell^{-2} & 0 & 12EI_\zeta\ell^{-3} & -6EI_\zeta\ell^{-2} \\ 0 & 6EI_\zeta\ell^{-2} & 2EI_\zeta\ell^{-1} & 0 & -6EI_\zeta\ell^{-2} & 4EI_\zeta\ell^{-1} \end{bmatrix}}_{\hat{\mathcal{K}}} \begin{bmatrix} f_0 \\ g_0 \\ \theta_0 \\ f_1 \\ g_1 \\ \theta_1 \end{bmatrix} = \begin{bmatrix} F_{\xi,0} \\ F_{\eta,0} \\ M_{\zeta,0} \\ F_{\xi,1} \\ F_{\eta,1} \\ M_{\zeta,1} \end{bmatrix}. \tag{3.22}$$

Before assembling the global system, we first need to map the displacements and forces of the reference truss $\hat{T}$ in the coordinate system $(\mathcal{O}, \xi, \eta, \zeta)$ to the truss T_m in the coordinate system $(\mathcal{O}, x, y, z)$.

3.2 Mapping from the reference truss to the trusses in the lattice

A lattice L is composed of a set T of trusses of arbitrary length and orientation. For each truss T_m, these two information are entirely determined by the nodes x_i and x_j, as illustrated in Figure 5. For a bidimensional lattice, the orientation of truss T_m is defined in terms of angle α_m, which is the angle between the x_1-axis and the non-deformed neutral axis of truss T_m (Figure 5). The connectivity $\mathcal{M}$ is usually employed to relate and order the nodes x_i and x_j to a specific truss T_m.

However, the connectivity $\mathcal{M}$ alone is not sufficient to relate the displacements and forces of the reference truss $\hat{T}$ to the truss T_m since they are not described in the same coordinate system. The mapping for a bidimensional lattice between the local displacement and rotation $\{f_0, g_0, \theta_0\}$ of the reference node $\hat{x}_0$ to the displacement and rotation $\{u_{x,i}, u_{y,i}, \phi_{z,i}\}$ of the node x_i in the global coordinate system is given by

$$\begin{bmatrix} \cos\alpha_m & \sin\alpha_m & 0 \\ -\sin\alpha_m & \cos\alpha_m & 0 \\ 0 & 0 & 1 \end{bmatrix} \begin{bmatrix} u_{x,i} \\ u_{y,i} \\ \phi_{z,i} \end{bmatrix} = \begin{bmatrix} f_0 \\ g_0 \\ \theta_0 \end{bmatrix} \tag{3.23}$$

The same orthogonal transformation is employed to map the forces and moments $\{F_{\xi,0}, F_{\eta,0}, M_{\zeta,0}\}$ applied at the reference node x_0 in the $(\mathcal{O}, \xi, \eta, \zeta)$ coordinate system to the force and moments

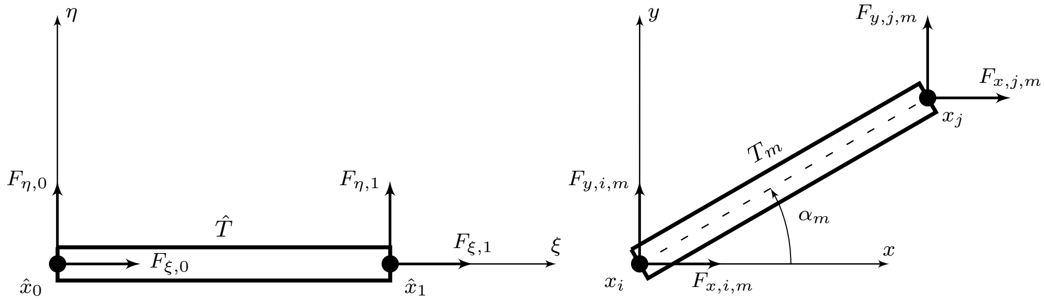

Figure 5: The reference truss $\hat{T}$ in its local coordinate system $(\mathcal{O}, \xi, \eta, \zeta)$ and the truss T_m in its global coordinate system $(\mathcal{O}, x, y, z)$

applied to the node x_i of truss T_m in the $(\mathcal{O}, x, y, z)$ coordinate system. These forces and moments are denoted $\{F_{x,i,m}, F_{y,i,m}, M_{z,i,m}\}$, where the indice m indicated that the forces and moments are applied to the truss T_m.

$$\underbrace{\begin{bmatrix} \cos\alpha_m & \sin\alpha_m & 0 \\ -\sin\alpha_m & \cos\alpha_m & 0 \\ 0 & 0 & 1 \end{bmatrix}}_{R_{\alpha_m}} \begin{bmatrix} F_{x,i,m} \\ F_{y,i,m} \\ M_{z,i,m} \end{bmatrix} = \begin{bmatrix} F_{\xi,0} \\ F_{\eta,0} \\ M_{\zeta,0} \end{bmatrix} \tag{3.24}$$

The reference equilibrium equations that relates the displacements and forces in the global coordinate system $(\mathcal{O}, x, y, z)$ can be written as

$$R_m^T \hat{\mathcal{K}} R_m \begin{bmatrix} u_{x,i} \\ \vdots \\ \phi_{z,j} \end{bmatrix} = \begin{bmatrix} F_{x,i,m} \\ \vdots \\ M_{z,j,m} \end{bmatrix}, \text{ where } R_m = \begin{bmatrix} R_{\alpha_m} & 0 \\ 0 & R_{\alpha_m} \end{bmatrix} \tag{3.25}$$

The procedure for a truly three dimensional lattice is similar but is not shown here in order to keep the exposition simple.

3.3 The global system of equations

The displacement field that minimizes the energy (3.1) of lattice L under the previous hypotheses regarding the geometry and the Euler-Bernoulli model must assure/ensure the equilibrium of forces and moments in the entire lattice. To this end, we enforce the balance of forces and moments on the set P of all points of lattice L.

We denote by $\mathcal{M}_i$ the connectivity of point x_i (the index of the trusses connected to x_i). We now differentiate the cases of interior node, boundary nodes on which tractions and moments are applied and boundary nodes subjected to Dirichlet boundary conditions. At each of the interior points $x_i \in P_I$, no external forces or moments are applied, hence the first set of equilibrium relations are written as (for a two dimensional lattice):

$$\sum_{m \in \mathcal{M}_i} F_{1,i,m} = 0, \qquad \forall x_i \in P_I, \tag{3.26a}$$

$$\sum_{m \in \mathcal{M}_i} F_{2,i,m} = 0, \qquad \forall x_i \in P_I, \tag{3.26b}$$

$$\sum_{m \in \mathcal{M}_i} M_{3,i,m} = 0, \qquad \forall x_i \in P_I. \tag{3.26c}$$

The equilibrium of force and moments must also be enforced at the boundary nodes. We denote by P_D the set of points $x_i \in P \setminus P_I$ where Dirichlet conditions are imposed ($u_{x,i} = u_{y,i} = \phi_{z,i} = 0$, $\forall x_i \in P_D$). We also denote by P_N the set of points $x_i \in P \setminus P_I$ where Neumann conditions are imposed. The second set of equilibrium relations are:

$$\sum_{m \in \mathcal{M}_i} F_{x,i,m} - F_{x,i,ext} = 0, \qquad \forall x_i \in P_N, \tag{3.27a}$$

$$\sum_{m \in \mathcal{M}_i} F_{y,i,m} - F_{y,i,ext} = 0, \qquad \forall x_i \in P_N, \tag{3.27b}$$

$$\sum_{m \in \mathcal{M}_i} M_{z,i,m} - M_{z,i,ext} = 0, \qquad \forall x_i \in P_N, \tag{3.27c}$$

where $F_{x,i,ext}$, $F_{y,i,ext}$ and $M_{z,i,ext}$ represent the external forces and moments applied to the node x_i. The last set of equations are given by the Dirichlet conditions:

$$u_{x,i} = 0, \qquad \forall x_i \in P_D, \tag{3.28a}$$

$$u_{y,i} = 0, \qquad \forall x_i \in P_D, \tag{3.28b}$$

$$\phi_{z,i} = 0, \qquad \forall x_i \in P_D. \tag{3.28c}$$

We denote by U the vector containing the displacements and rotations of all points $x_i \in P$. We denote by $\mathcal{U}$ the set of admissible displacements of the set of points P. More precisely, the set of displacements must satisfy the Dirichlet conditions (3.28) ($\mathcal{U} = \{U \in \mathbb{R}^{3N_P} \,|\, u_{x,i} = u_{y,i} = \phi_{z,i} = 0, \forall x_i \in P_D\}$). This definition can also be easily extended to three dimensional lattice. The variables U and P are sometimes referred as the state and control variables respectively. We also denote by F the vector containing the force and moments applied at all node $x_i \in P$ (the forces and moments are null for all $x_i \in P_I \cup P_D$). The set of equilibrium equations (3.26), (3.27) and Dirichlet conditions (3.28) can be conveniently recast in the global system of equations:

$$e(U,P) := \mathcal{K}(P)U - F = 0, \tag{3.29}$$

where $\mathcal{K}$ is the resulting stiffness matrix. We also denote by $\mathcal{D}$ the set of admissible set of points P. More precisely, we want a set P of points that possess distinct points that lie in the closure of Ω

($\mathcal{D} = \{P \,|\, \forall x_i, x_j \in P, x_i, x_j \in \bar{\Omega}$ and $x_i \neq x_j$ for $i \neq j\}$). The restriction that the nodes must be distinct is necessary to ensure that the equilibrium relation e and the strain energy $\mathcal{E}$ are well-defined. It is important to note that as long the set P of nodes belongs to $\mathcal{D}$ and that at least a Dirichlet condition is applied to one point ($P_D \neq \varnothing$), the stiffness matrix $\mathcal{K}$ is invertible. Hence, for a given set P of points, the displacements U satisfying (3.29) is unique. The imposition of at least one Dirichlet condition can also be relate to constraint the motion of a lattice.

Once the solution U is computed, the displacement field over the entire lattice is known through the equations (3.19) and (3.23). The strain energy $\mathcal{E}_{T_m}$ of each truss T_m can therefore be obtained through (3.13) as well as the total strain energy $\mathcal{E}$ of the lattice by computing

$$\mathcal{E}(U, P) = \sum_{m=1}^{N_T} \mathcal{E}_{T_m}(U, P). \tag{3.30}$$

We now analyze the properties of the system of equations $e(U, P) = 0$. We will note the partial directional derivative of e by $\partial_U e(U, P)(\delta U)$ and by $\partial_P e(U, P)(\delta P)$ along the directions δU and δP respectively. **Il faut vérifier que e est continuously Frechet differentiable pour appliquer le theorème de la fonction implicite.** Since the application e is continuously Frechet differentiable on $\mathcal{U} \times \mathcal{P}$ and that $\partial_U e(U, P)$ **is an invertible linear application**, we can apply the Implicit Function Theorem which state that there exist a unique continuous function

$$\begin{aligned} w: \;\; & \mathcal{D} \to \mathcal{U} \\ & P \mapsto w(P) = U \end{aligned} \tag{3.31}$$

such that $e(U, P) = e(w(P), P) = 0$. Although we know that w exists, the analytic expression may not be known. However, in our case, the function w is known and is given by $w(P) = \mathcal{K}^{-1}(P)F$. Also, the total strain energy $\mathcal{E}$ of a lattice L can be described solely with the variable P. For the sake of clarity, we will note:

$$\hat{\mathcal{E}}(P) := \mathcal{E}(w(P), P) = \mathcal{E}(\mathcal{K}^{-1}(P)F, P). \tag{3.32}$$

Again, for each $P \in \mathcal{D}$, one can compute $\hat{\mathcal{E}}(P)$. We will note $D\hat{\mathcal{E}}(P)(\delta P)$ the total directional derivative of $\hat{\mathcal{E}}$ evaluated at P in the direction δP. It is important to note that a dimensionless equilibrium relation e and strain energy $\hat{\mathcal{E}}$ are computed in order to obtain well-scaled optimization problems that will be described in the next section.

4 Formulations of the Shape Optimization Problems

We present in this section two formulations of the shape optimization problem and introduce equilibrium and geometrical constraints that we shall consider. The reduced problem is employed in order to remove the state variable U from the optimization problems. Then, we present the interior-point method that will be used for the solution of the finite-dimensional optimization problems. Finally, the adjoint problem is introduced in order to efficiently compute the derivative information.

The common objective of the various formulations of the shape optimization problem is to seek the set $P \in \mathcal{D}$ of a lattice L such that its strain energy $\mathcal{E}$ is minimized. The first, and maybe the simplest, formulation of the shape optimization problem is the one where the boundary nodes $P_i \in P_{\Gamma_k}$ are constrained to remain on Γ_k. We describe each boundary Γ_k with a function $\gamma_k \in C^\infty(\mathbb{R}^d)$ such that $\gamma_k(x_i) = 0$, $\forall x_i \in P_{\Gamma_k}$ and $\gamma_k(x_i) \neq 0$ everywhere else. The first shape optimization is formulated as follows

$$\text{Problem with } \Gamma \text{ constraint} \qquad \begin{array}{cl} \min\limits_{U \in \mathcal{U}, P \in \mathcal{D}} & \mathcal{E}(U,P), \\ \text{s.t.} & e(U,P) = 0, \\ & \gamma_k(x_i) = 0, \quad \forall x_i \in P_{\Gamma_k}, k = 1, \dots, N_\Gamma. \end{array} \tag{4.1}$$

It is important to observe that the displacement field $U \in \mathcal{U}$ is also a variable of the optimization problem since the strain energy $\mathcal{E}$ depends on U. By using (4.1), a new formulation of the optimization problem, sometimes referred to as the reduced problem, can be formulated as follows

$$\text{Reduced problem with } \Gamma \text{ constraint} \qquad \begin{array}{cl} \min\limits_{P \in \mathcal{D}} & \hat{\mathcal{E}}(P), \\ \text{s.t.} & \gamma_k(x_i) = 0, \quad \forall x_i \in P_{\Gamma_k}, k = 1, \dots, N_\Gamma. \end{array} \tag{4.2}$$

This reduced formulation only possess the set P of points as variables and the equilibrium relation $e(U,P)$ is readily satisfy for each $P \in \mathcal{D}$. For this work, only the reduced version of the optimization problems will be considered due to its computational cost, as it will be explained below.

We can add a geometrical constraint to problem (4.2) to force the truss T_j to be arranged as near-equilateral elements through the constraint c_κ (the impact of the choice of the lower bound ρ will be analyzed in Section 5).

$$\text{Reduced problem with } (\Gamma, K) \text{ constraint} \qquad \begin{array}{cl} \min\limits_{P \in \mathcal{D}} & \hat{\mathcal{E}}(P) \\ \text{s.t.} & \gamma_k(x_i) = 0, \quad \forall x_i \in P_{\Gamma_k}, k = 1, \dots, N_\Gamma, \\ & \rho \leq c_\kappa(K_e) \quad e = 1, \dots, N_K \end{array} \tag{4.3}$$

The elements K_e do not constitute separate variables of the shape optimization problem (4.3) since these elements are entirely defined by the set P of points. Since the set P is of finite dimension, the precedent shape optimization problems consist of finite dimensional optimization problems. We now present the methodology employed to solve these three shape optimization problems.

4.1 Interior-Point Method

To solve the different shape optimization problems, we employ the open-source solver IPOPT that implements an interior-point method. The choice of the solver IPOPT is motivated by the fact that it can handle finite dimensional optimization problems with non-linear equality and inequality constraints as well as non-linear and non-convex objective functions. We briefly present here the implementation of the interior-point method in IPOPT. A more thorough description of this particular solver is done in [22, 23] and an extensive presentation is available in [15, Chapter 19]. Without loss of generality, we introduce the interior-point method on the shape optimization problem (4.3). The method first introduces slack variables $s \in \mathbb{R}^{N_K}$ to produce the following problem:

$$\begin{array}{lll} \min\limits_{P\in\mathcal{D}, s\in\mathbb{R}^{N_K}} & \hat{\mathcal{E}}(P), & \\ \text{s.t.} & \gamma_k(x_i) = 0, & \forall x_i \in P_{\Gamma_k}, k = 1,\dots,N_\Gamma, \\ & c_\kappa(K_e) - \rho - s_e = 0 & e = 1,\dots,N_K, \\ & s_e \geq 0 & e = 1,\dots,N_K. \end{array} \tag{4.4}$$

For the sake of clarity, we will note $c_{\mathbb{E}}(P)$ the function containing all the constraints on the boundary nodes and $c_{\mathbb{I}}(P)$ the function containing all the constraint on the quality of the elements K_e. With a slight abuse of notation, $s \geq 0$ represents a component-wise inequality. The problem (4.4) can be simplified as follows:

$$\begin{array}{ll} \min\limits_{P\in\mathcal{D}, s\in\mathbb{R}^{N_K}} & \hat{\mathcal{E}}(P), \\ & c_{\mathbb{E}}(P) = 0, \\ & c_{\mathbb{I}}(P) - s = 0, \\ & s \geq 0. \end{array} \tag{4.5}$$

Let $\lambda_{\mathbb{E}}$ be the Lagrange multiplier associated with the equality constraints (the constraints on the points on the boundary) and $\lambda_{\mathbb{I}}$ the Lagrange multiplier associated with the inequality constraints (the constraints on the quality of the elements K_e). We then introduce the Lagrangian functional of problem (4.5):

$$\mathcal{L}(P, \lambda_{\mathbb{E}}, \lambda_{\mathbb{I}}) = \hat{\mathcal{E}}(P) - \lambda_{\mathbb{E}}^T c_{\mathbb{E}}(P) - \lambda_{\mathbb{I}}^T c_{\mathbb{I}}(P). \tag{4.6}$$

We shall use the Karush-Kuhn-Tucker (KKT) conditions, which provide necessary first order conditions that a local minimum must satisfy.

$$\nabla_P \mathcal{L}(P, \lambda_{\mathbb{E}}, \lambda_{\mathbb{I}}) = \nabla_P \hat{\mathcal{E}}(P) - \nabla_P {c_{\mathbb{E}}}^T(P)\lambda_{\mathbb{E}} - \nabla_P {c_{\mathbb{I}}}^T(P)\lambda_{\mathbb{I}} = 0 \tag{4.7a}$$

$$c_{\mathbb{E}}(P) = 0 \tag{4.7b}$$

$$c_{\mathbb{I}}(P) - s = 0 \tag{4.7c}$$

$$S\lambda_{\mathbb{I}} = 0 \tag{4.7d}$$

$$s, \lambda_{\mathbb{I}} \geq 0 \tag{4.7e}$$

As shown with the early results presented in Section 4, the objective function $\hat{\mathcal{E}}$ can be non-convex, hence possessing multiple local minima. Since the interior-point method described here only seeks a solution that respects the KKT conditions, it can happen that a local minima rather than a global minima be reached. The interior-point method consists in relaxing the complementarity condition (4.7d) with a positive parameter μ in order to circumvent the problem of presuming which inequality constraint is active or not. This parameter μ is decreased through the optimization procedure in order to approach a solution satisfying (4.7). One can adopt essentially two methodologies to adapt this parameter, the Fiacco-McCormick strategy or an adaptive strategy. The interested reader can refer to [14] and [15, Chapter 19] for a detailed description of these approach.

The relaxation of the complementarity conditions (4.7d) to (4.8d) can also be regarded as a way to remove the inequality constraint on the slack variable s by adding a logarithmic barrier to the objective function. The modified KKT conditions are then:

$$\nabla_P \mathcal{L}(P, \lambda_{\mathbb{E}}, \lambda_{\mathbb{I}}) = \nabla_P \hat{\mathcal{E}}(P) - \nabla_P {c_{\mathbb{E}}}^T(P)\lambda_{\mathbb{E}} - \nabla_P {c_{\mathbb{I}}}^T(P)\lambda_{\mathbb{I}} = 0 \tag{4.8a}$$

$$c_{\mathbb{E}}(P) = 0 \tag{4.8b}$$

$$c_{\mathbb{I}}(P) - s = 0 \tag{4.8c}$$

$$S\lambda_{\mathbb{I}} - \mu = 0 \tag{4.8d}$$

$$s, \lambda_{\mathbb{I}} \geq 0 \tag{4.8e}$$

To find a solution P that satisfy (4.8) for a sufficiently small μ, the IPOPT solver employ a line search approach. Starting with a initial approximation $(P^0, s^0, \lambda_{\mathbb{E}}^0, \lambda_{\mathbb{I}}^0)$, a next iterate is computed according to:

$$P^{k+1} = P^k + \alpha d_P, \tag{4.9a}$$

$$s^{k+1} = s^k + \alpha_s d_s, \tag{4.9b}$$

$$\lambda_{\mathbb{E}}^{k+1} = \lambda_{\mathbb{E}}^k + \alpha d_{\mathbb{E}}, \tag{4.9c}$$

$$\lambda_{\mathbb{I}}^{k+1} = \lambda_{\mathbb{I}}^k + \alpha d_{\mathbb{I}}. \tag{4.9d}$$

To compute the directions d_P, $d_{\mathbb{E}}$, $d_{\mathbb{I}}$, and d_s, the Newton method is applied to (4.8). The linear system obtained is called the primal-dual system.

$$\begin{bmatrix} \nabla_{PP}\mathcal{L}(P^k, s^k, \lambda_{\mathbb{E}}^k, \lambda_{\mathbb{I}}^k) & 0 & -\nabla_P {c_{\mathbb{E}}}^T(P^k) & -\nabla_P {c_{\mathbb{I}}}^T(P^k) \\ 0 & \mathit{\Lambda}_{\mathbb{I}} & 0 & S \\ -\nabla_P c_{\mathbb{E}}(P^k) & 0 & 0 & 0 \\ -\nabla_P c_{\mathbb{I}}(P^k) & -I & 0 & 0 \end{bmatrix} \begin{bmatrix} d_P \\ d_s \\ d_{\mathbb{E}} \\ d_{\mathbb{I}} \end{bmatrix} = \begin{bmatrix} \nabla_P \mathcal{L}(P^k, s^k, \lambda_{\mathbb{E}}^k, \lambda_{\mathbb{I}}^k) \\ S\lambda_{\mathbb{I}} - \mu \\ c_{\mathbb{E}}(P^k) \\ c_{\mathbb{I}}(P^k) - s \end{bmatrix} \tag{4.10}$$

As mentioned in Section 4, working with the reduced shape optimization problem (4.2) and (4.3) allows for the reduction of the size of the linear system (4.10), hence decreasing the computational cost of calculating each iterate. Once the directions d are computed, the step length α and α_s are **calculated by means** of filters. **These filters check if the next iterate obtained reduce the objective function without increasing the constraint violation ($\|c_{\mathbb{E}}(P^{k+1}), c_{\mathbb{I}}(P^{k+1})\|$) and the other way around**. A more complete description of these filters and on how the system (4.10) is solved are again presented in [15, 23].

4.2 Derivative Information and Adjoint Problem

As shown previously, the interior-point method requires the information of the **gradient** of the Lagrangian function $\mathcal{L}$ and its hessian. The latter is not computed exactly, but rather a Quasi-Newton method, namely the BFGS approximation, is employed [15, Chapter 6]. To ensure the convergence of the interior-point method, exact knowledge of the **gradient** of the Lagrangian $\mathcal{L}$, in particular the **gradient** of the objective function $\hat{\mathcal{E}}$, is however needed. The computation of the **total derivative** of the objective function $\hat{\mathcal{E}}$ can be done efficiently by employing **the/an** adjoint problem. The **forthcoming** description follows essentially the one presented in the manuscript [10]. We first compute the total directional derivative $D\hat{\mathcal{E}}(P)(\delta P)$ by noting the duality pairing $\langle \cdot, \cdot \rangle$:

$$\langle D\hat{\mathcal{E}}(P), \delta P\rangle_{\mathcal{D}^*,\mathcal{D}} = \langle D\mathcal{E}(w(P), P), \delta P\rangle_{\mathcal{D}^*,\mathcal{D}}, \tag{4.11a}$$

$$= \langle \partial_U \mathcal{E}(w(P), P), Dw(P)(\delta P)\rangle_{\mathcal{U}^*,\mathcal{U}} + \langle \partial_P \mathcal{E}(w(P), P), \delta P\rangle_{\mathcal{D}^*,\mathcal{D}}, \tag{4.11b}$$

$$= \langle Dw(P)^* \partial_U \mathcal{E}(w(P), P), \delta P\rangle_{\mathcal{D}^*,\mathcal{D}} + \langle \partial_P \mathcal{E}(w(P), P), \delta P\rangle_{\mathcal{D}^*,\mathcal{D}}. \tag{4.11c}$$

Since the total derivative is needed and not only the directional derivative in the direction δP, we can obtain from the previous equations:

$$D\hat{\mathcal{E}}(P) = Dw(P)^* \partial_U \mathcal{E}(w(P), P) + \partial_P \mathcal{E}(w(P), P). \tag{4.12}$$

As mentioned in Section 3 the function w may not be known, hence the dual operator $Dw(P)^*$ can not be computed. We use again the Implicit Function Theorem to circumvent this problem. Another **result** of the Implicit Function Theorem provides the needed information regarding the derivative of w **(Ajouter plus de détails?)**:

$$Dw(P) = -\partial_U e(w(P), P)^{-1}\, \partial_P e(w(P), P). \tag{4.13}$$

The total derivative $D\hat{\mathcal{E}}(P)$ can then be computed this way:

$$D\hat{\mathcal{E}}(P) = -\partial_P e(w(P), P)^*\, \partial_U e(w(P), P)^{-*}\, \partial_U \mathcal{E}(w(P), P) + \partial_P \mathcal{E}(w(P), P). \tag{4.14}$$

The adjoint problem consist in solving **the linear system** $\partial_U e(w(P), P)^* q = -\partial_U \mathcal{E}(w(P), P)$. Once the quantity p is calculated, the total derivative is computed:

$$D\hat{\mathcal{E}}(P) = -\partial_P e(w(P), P)^*\, q + \partial_P \mathcal{E}(w(P), P). \tag{4.15}$$

Once the total derivative is known, the gradient $\nabla_P \hat{\mathcal{E}}$ can readily be obtained. It is important to note that the use of the adjoint problem to **acquire** $D\hat{\mathcal{E}}(P)$ is advantageous compared to the use of finite differences. In fact, the adjoint method need only to solve one linear system, whereas the use of finite differences necessitate the resolution of the equilibrium relation $e(U, P+\delta P) = 0$ for each δP chosen (a minimum of N_P perturbation δP are necessary). Moreover, the derivative information obtained via finite difference consist only in approximation while the precedent methodology gives the exact derivative information. Finally, the gradient on the equality constraints $\nabla_P c_{\mathbb{E}}(P)$ and on the inequality constraints $\nabla_P c_{\mathbb{I}}(P)$ are computed directly since they do not depend on U. **Faut-il ajouter un schéma/algorithme montrant les interations entre le solveur IPOPT et le forward problem?**

5 Numerical Examples

We present in this section various formulations of the shape optimization problem and we solve these problems on simple test cases. We analyze the performance of each formulation with respect to the functional objective and we identify geometrical inconsistencies in the solution. We also discuss theoretically the existence, and sometimes the non-existence, and uniqueness of solutions of the shape optimization problems.

5.1 Existence of Solutions

We consider for all numerical examples shown in this section that the dimensionless values of the radius of the trusses, their Young modulus E and the norm of the external forces ($\|F_{ext}\|$) are equal to one.

We first investigate the existence of solutions of the shape optimization problems (4.2) and (4.3) for the problem illustrated in Figure 6. The right side of this Figure 6 presents a lattice extracted from the geometry Ω_1. We assume that the width and height of Ω_1 possess the dimensionless value of 100. Hence, the dimensionless position of nodes x_1 and x_3 are $(0, 0)$ and $(100, 100)$ respectively.

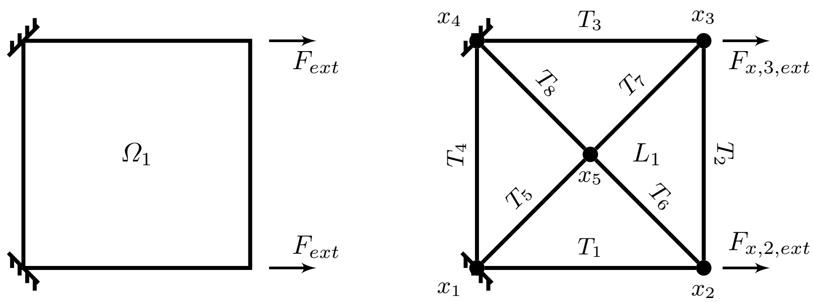

Figure 6: Geometry Ω_1 with its loadings (left) and a corresponding lattice L_1 (right).

For the lattice illustrated in Figure 6, only the position of the node x_5 is a control variable In order to assess whether there exists a solution or not, we analyze the level-set of the objective function and the feasible region for both shape optimization problems (4.2) and (4.3).

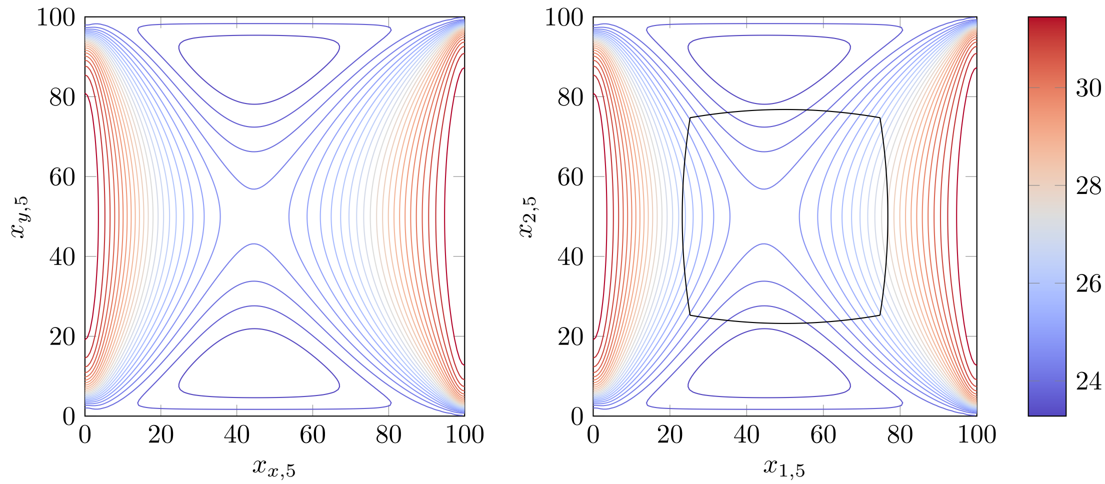

Figure 7: Level-set of the strain energy for the shape optimization problem (4.2) (left) and (4.3) (right) on the first example. The feasible region for the problem (4.2) is the interior of the whole square, while the feasible region for the problem (4.3), with a lower bound $\rho = 0.5$, is limited to the inside curved box with the black boundary. Because both problems (4.2) and (4.3) possess the same objective function (the strain energy), their level-set are identical.

We observe in Figure 7 that the strain energy of the lattice L_1 is nonlinear (as mentioned in Section 3.3) with respect to the position of the node x_5. Moreover, the objective functional is not convex **and the optimal lattice structure is not symmetric although the loading is.** The optimal lattice obtained for the shape optimization problems (4.2) and (4.3) are presented in Figure 8. The dimensionless strain energy for each optimized lattice **is/are** presented in Table 1. The initial lattice is the one described in Figure 6. As expected, the strain energy of the lattice obtained with problem (4.2) is smaller than the strain energy of the lattice obtained with problem (4.3) since the feasible region of the latter is included in that of the former.

Table 1: Comparison of the strain energy for lattice L_1

	Initial lattice	Optimized lattice with problem (4.2)	Optimized lattice with problem (4.3)
Strain energy	24.4733	22.9407	23.3621

We now verify on a second simple problem if the previous observations hold true. The second geometry and loadings to be studied are shown in Figure 9. The length of each side of the equilateral triangle has the dimensionless value of 100.

For this second problem, the position of the node x_4 constitutes the variable of the shape optimization problem. Once again, the level-set of the strain energy and the feasible region for

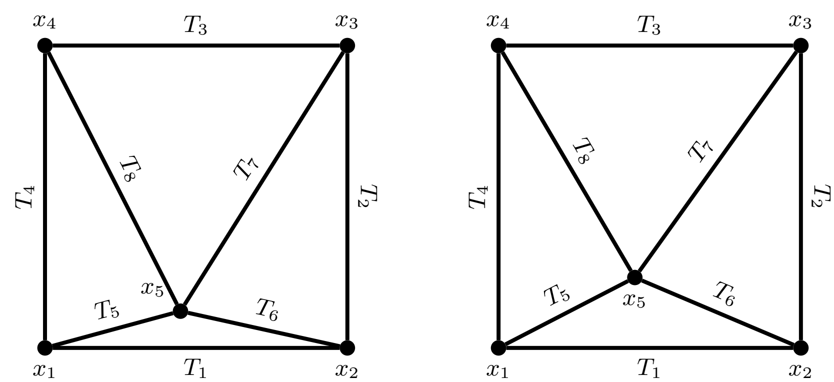

Figure 8: Optimized lattice with the problem (4.2) (left) and with the problem (4.3) (right) for the first example.

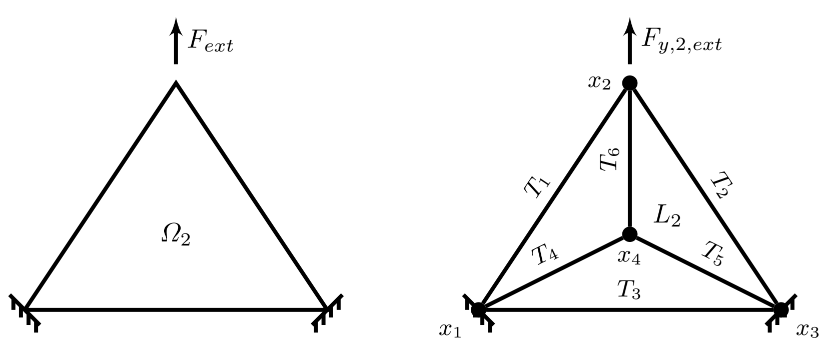

Figure 9: Geometry Ω_2 with its loadings (left) and a corresponding lattice L_2 (right).

problems (4.2) and (4.3) are presented in Figure 10

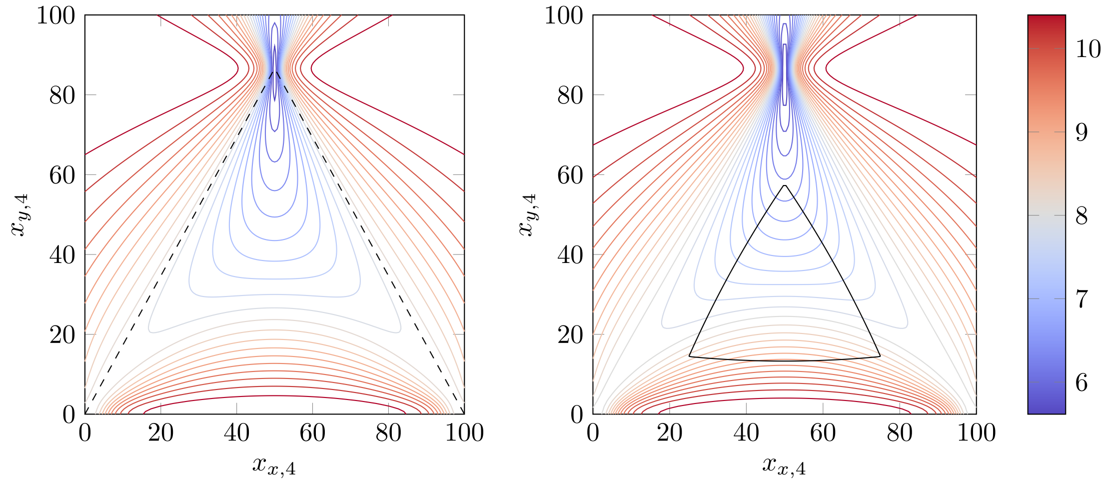

Figure 10: Level-set of the strain energy for the shape optimization problem (4.2) (left) and (4.3) (right) for the second example. The feasible region for the problem (4.2) is the interior of the whole equilateral triangle. The feasible region for the problem (4.3) with $\rho = 0.5$ is the triangular-shaped domain and its interior.

We observe in Figure 10 that there exist no minima for the shape optimization problem (4.2) in the feasible region. Indeed, the position of the node x_4 that minimize the strain energy of lattice L_2 is exactly at the position of the node x_2 (Figure 9). This particular position is not included in $\mathcal{D}$, therefore the shape optimization (4.2) has no solution. On the other hand, the problem (4.3) is well-posed since the quality constraint on the elements makes the feasible set closed. As the level-set in Figure 10 shows, the minima is located in the top corner of the triangular shape.

We present a third simple example to verify if the quality constraints c_κ of problem (4.3) can lead to some geometrical inconsistencies. This third example is a slight variation of the previous one; the geometry and the loading, as well as the corresponding lattice, are presented in Figure 11.

For this problem, we consider that the width and the height of the triangular shape is a dimensionless length of 100 and that the control variable is the position of the node P_4. Once again, the level-set and the feasible regions are shown in Figure 12 for the shape optimization problem (4.2) and (4.3).

Just as in the second example, the shape optimization problem (4.2) for the lattice L_3 does not possess a minima since the feasible region for this problem is an open subset of $\mathbb{R}^2$. For the shape optimization problem (4.3), a solution does exist since the feasible region is a closed subset of $\mathbb{R}^2$ (the region described by the solid line). However, the region delimited by the dotted line is also a **zone** where the quality constraint $\rho \leq c_\kappa(K_e)$, $e = 1, \ldots, 3$ is respected. Since the constraint $P \in \mathcal{D}$

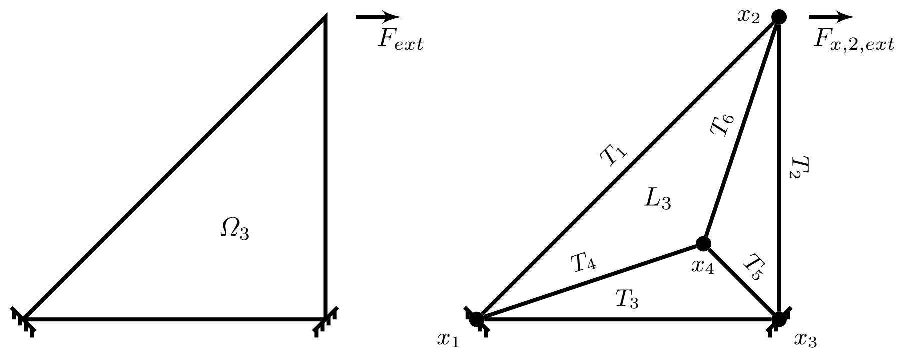

Figure 11: Geometry Ω_3 with its loadings (left) and a corresponding lattice L_3 (right).

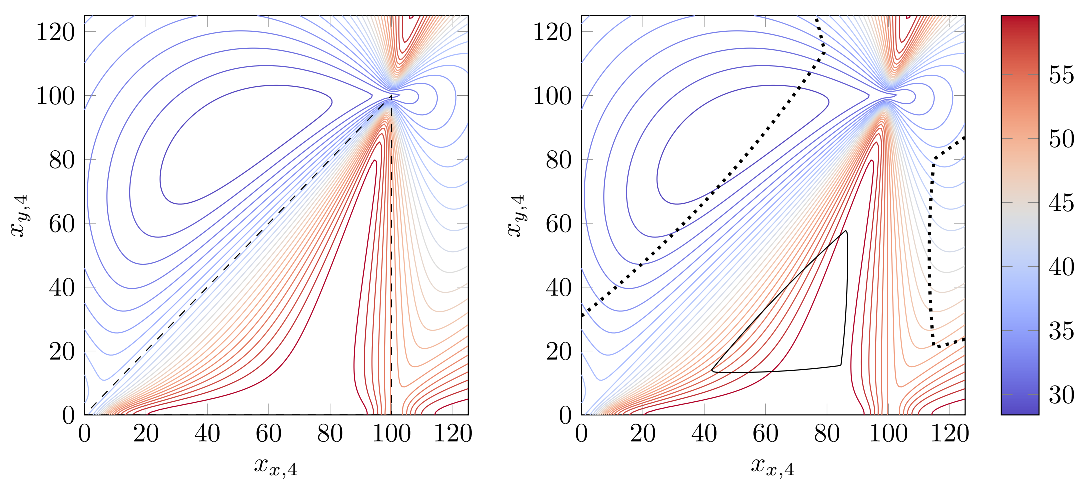

Figure 12: Level-set of the strain energy for the shape optimization problem (4.2) (left) and (4.3) (right) on the third example. The feasible region for the problem (4.2) is the interior of the whole isosceles triangle. The feasible region for the problem (4.3) with $\rho = 0.3$ is the triangular-shaped delimited by the solid line and its interior. The two regions delimited by the dotted lines are **zones** where the constraint $\rho \le c_\kappa(K_e), e = 1, \ldots, 3$ is also respected.

is not explicitly enforced and that the method employed to solve the optimization problem uses a line-search technique, it is possible to find a minima that is outside of the prescribed domain Ω_3. When this particular case occurs, one or multiples elements K_e of the lattice happen to be flipped. Not only this **phenomena** may cause the nodes to move outside of the feasible region, but it can also produce crossing of trusses where there is no nodes. The right lattice of Figure 13 presents an optimal lattice that respect $P \in \mathcal{D}$ while the left lattice present a lattice with node x_4 outside of the feasible region, hence $P \notin \mathcal{D}$.

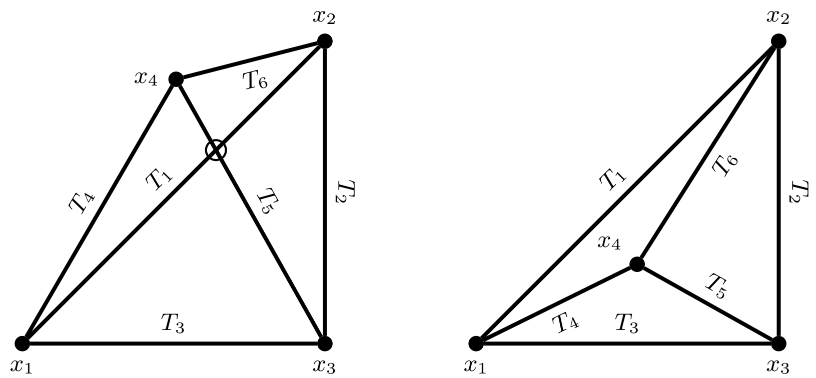

Figure 13: Non-acceptable optimal lattice (left) since the node x_4 does not lies in $\bar{\Omega}$. Acceptable optimal lattice for the third example (right) where the node x_4 is in $\bar{\Omega}$.

In order to prevent the shape optimization problem (4.3) to compute a lattice that does not respect the constraint $P \in \mathcal{D}$ or possess crossing of trusses, we penalize the constraint on the quality of the element c_κ where a particular element is flipped. By enforcing simultaneously the constraint γ on the boundary and the constraint c_κ on the quality of the element, the constraint $P \in \mathcal{D}$ is implicit respected.

As demonstrated with the simple examples 2 and 3, the shape optimization problem (4.2) does not always possess a minima. This is caused, as mentioned earlier, by the fact that the feasible region ($\mathcal{D}$ for this shape optimization problem) is not closed. One can argue that instead of finding the position of the set P of nodes in the set of set distinct nodes $\mathcal{D}$, the position of the nodes can be find in $\bar{\mathcal{D}}$. However, this closed subset will allow the nodes to be stacked, which will lead to a degenerated physical model of the lattice, because some trusses will possess a null length. Moreover, the nodes can be placed on the boundary $\partial\Omega$, hence resulting in the superposition of several trusses. Due to these observations, the shape optimization problem (4.2) will no longer be considered. For now on, only the shape optimization problem (4.3) will be employed since imposing simultaneously the boundary constraints and the quality constraints (along with the orientation of the elements) prevent any degeneracy of the physical model of lattice and also prevent geometrical inconsistency. **Mentionner toutefois que cela ne gatrantie pas nécessairement l'existence**

d’une solution, mais que ce problème semble toujours en posséder une.

5.2 Efficiency of the shape optimization problem (4.3)

We first check the efficiency of the shape optimization problem (4.2) by analyzing the reduction of the total and local strain energy. We consider the fourth simple example presented in Figure 14.

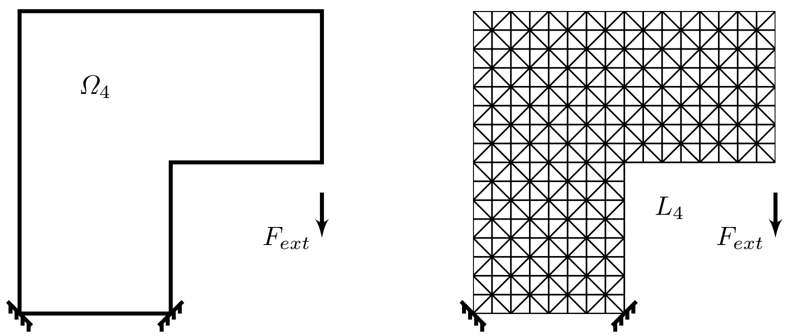

Figure 14: Geometry Ω_4 and loading of the fourth simple example (left) and the corresponding lattice L_4. For the sake of clarity, the nodes and the trusses are not labeled.

The width and the height of the L-shaped geometry are set to 200. The lower bound ρ on the quality of the elements is fixed to 0.5. The impact of this particular choice of lower bound ρ will be examined later. There is 450 control variables (225 nodes) for this example. The shape optimization problem (4.3) is applied to the lattice L_4 in order to obtain the set P of position of points such that the strain energy of the entire lattice attained a local minima. The optimal geometry is displayed in Figure 15 (right).

Multiples remarks can be made regarding the results presented in Figure 15. First, we observe that the optimal lattice $L_{4,opt}$ indeed possess a strain energy that is significantly reduce compared to the initial lattice L_4 (a diminution of approximately 50%). Second, the shape optimization problem (4.3) had transformed the structured lattice L_4 into a lattice that is clearly not structured. In fact, the trusses and nodes **tend** to be arranged in a sort of arch while some others tend to be concentrated at the corner of the L-shaped structure. Finally, we note that the maximum strain energy that a truss possess is also significantly reduce between the initial and the optimized lattice.

As mentioned previously, the lower bound ρ of the quality of the elements was arbitrary fixed to 0.5. We now investigate the impact of this lower bound ρ on the shape optimization problem (4.3) and hence the optimal lattice obtained. We consider the same example and lattice L_4 presented at Figure 14 with the same height and width of 200.

We observe in Figure 16 that the optimized lattices obtained with small lower bound ρ on the quality of the element possess nearly degenerated elements. On the other hand, the optimized lattice obtained with a greater lower bound tend to produce geometry whose element are nearly

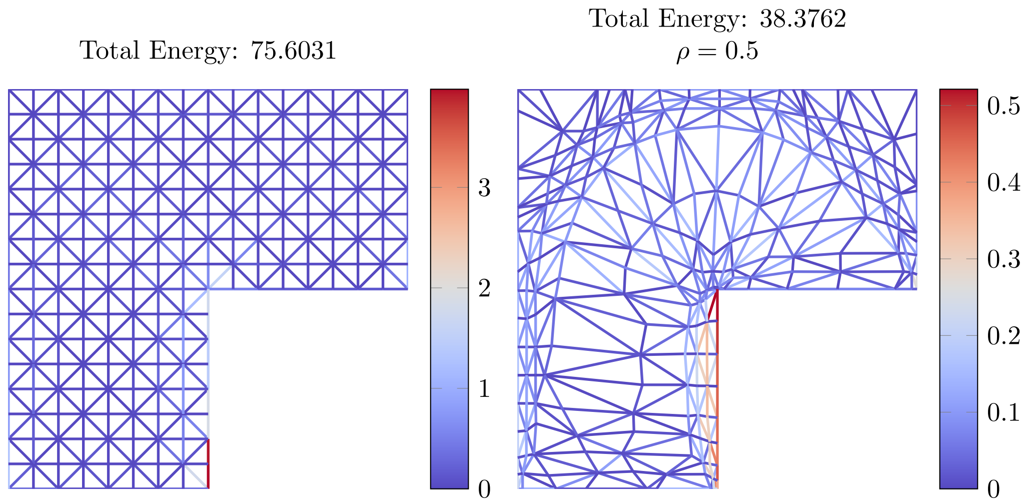

Figure 15: Initial lattice L_4 (left) and optimized lattice $L_{4,opt}$ (right). The local strain energy of each truss are indicated with the colorbar.

equilateral. The analysis of the strain energy of each optimized lattice show, as expected, that a larger lower bound ρ on the quality of the elements restrict significantly the feasible region of the shape optimization problem (4.3). For small lower bound, a minima for the shape optimization problem (4.3) can thus be seek in a wider feasible region. This explains the fact that the objective function (the strain energy $\hat{\mathcal{E}}$) is smaller for lower bounds $\rho \to 0$. We also remark as mentioned previously, that the nodes x_i (and then the trusses T_m) of the optimized lattices move in order to create an arch. **Discuter du pourquoi ne pas toujours prendre un petit ρ.**

For all the previous example, the lattice L_1 to L_4 where somewhat arbitrary extracted from the geometries Ω_1 to Ω_4. We now look into this process of creating an initial lattice from a geometry and assess whether or not it impacts the optimized lattice obtained. We consider again the geometry Ω_4 and we extract 2 different lattices L_4' and L_4'' possessing approximately the same number of nodes x_i (225 and 224 respectively) but with a different connectivity for their trusses. These two new lattices are presented in Figure 17.

We apply the shape optimization problem (4.3) on the lattices L_4' and L_4'' to obtain the optimal lattices displayed in Figure 18 (the lower bound ρ on the quality of the elements K_e is set to 0.6).

The same geometrical pattern of an arch can be observed in the optimal lattices displayed in Figure 18. While the overall appearance of these optimized structure remain the same, we can observe small variation in the strain energy. Since the connectivity of the lattice L_4, L_4' and L_4'' **is/are** different, the number of trusses T_m are also different for each lattice. We therefore analyze, for a fixed value of the lower bound ρ, the influence of the volume (see Definition 1) of the optimized lattices $L_{4,opt}$, $L_{4,opt}'$ and $L_{4,opt}''$ on their strain energy.

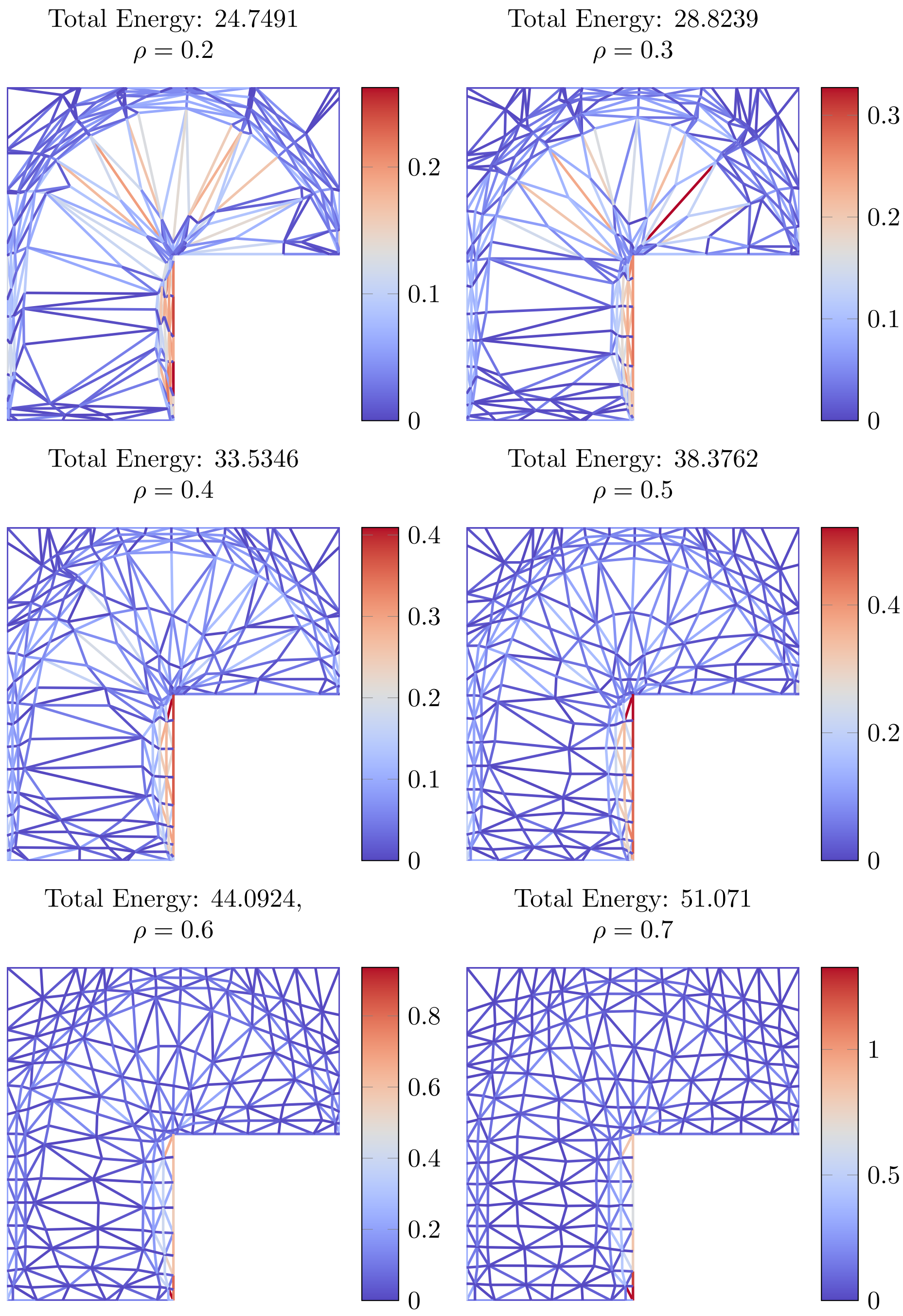

Figure 16: Optimized lattices $L_{4,opt}$ for the fourth example with various lower bound ρ on the quality of the elements.

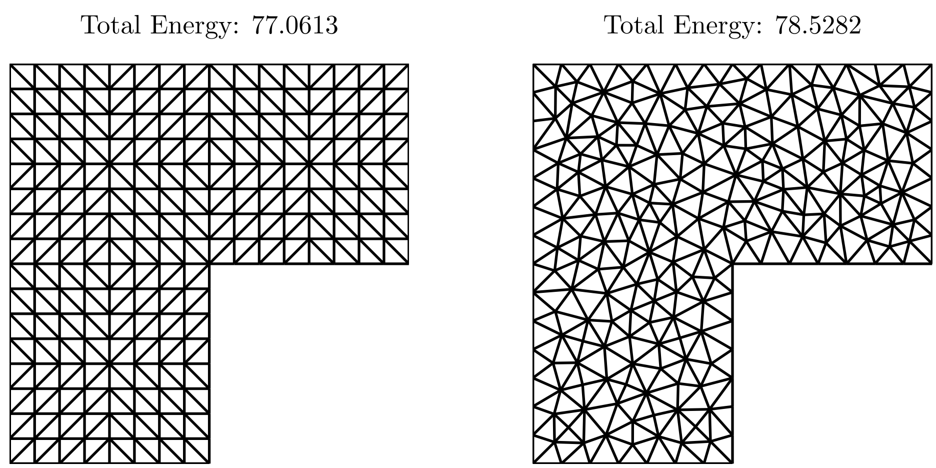

Figure 17: Alternative initial lattices L'_4 (left) and L''_4 (right) for the geometry Ω_4.

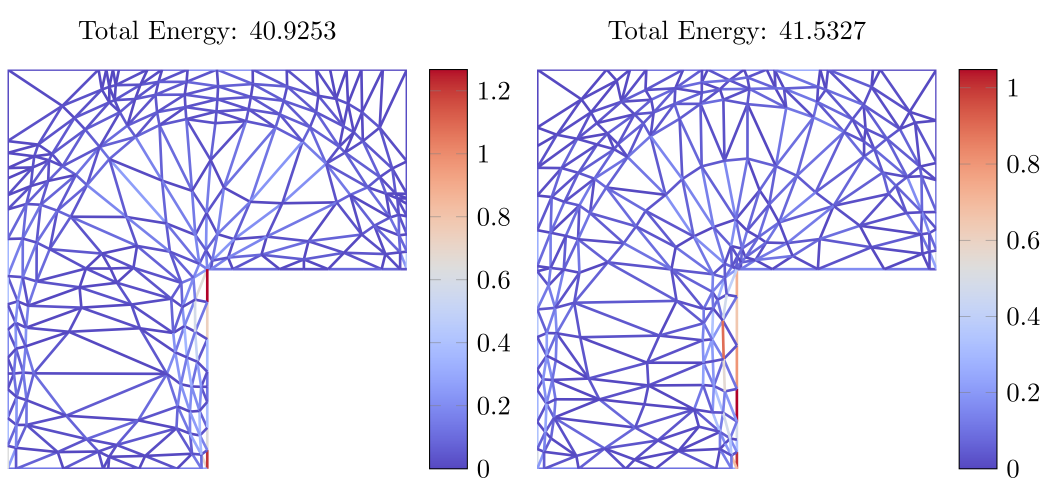

Figure 18: Optimized lattices $L'_{4,opt}$ (left) and $L''_{4,opt}$ (right) with their respective total and local strain energy.

Table 2: Volume and strain energy for the optimized lattices $L_{4,opt}$, $L'_{4,opt}$ and $L''_{4,opt}$

	Lattice $L_{4,opt}$	Lattice $L'_{4,opt}$	Lattice $L''_{4,opt}$
Volume	27 989	27 603	27 726
Strain energy	44.0924	40.9253	41.5327

We observe in Table 2 that, for similar value of volume, there is some variation in the strain energy of the optimized lattices. Also, the results presented in Table 2 indicate that the initial structured lattices (L_4 and L'_4) do not necessarily produce the best optimized lattice. All these observations suggest that the initial lattice, especially the connectivity $\mathcal{M}$ of its points x_i, impact the quality of the optimized lattice computed by solving the shape optimization problem (4.3). However, finding *a priori* an optimal connectivity $\mathcal{M}$ of the points x_i is an intractable problem, especially for lattice possessing à large number of points.

6 Conclusion

We have presented a new methodology aimed for the shape optimization of lattice produced by additive manufacturing technologies. A geometrical description of a lattice based on a polyhedral conforming meshing of a domain Ω is made. A general framework describes the mechanic of a lattice, then hypothesis are posed to model each trusses as Euler-Bernoulli beams. Two shape optimization problems exploit the consistent geometrical and physical description in order to seek the position of the nodes (and the trusses) that minimizes the strain energy of a lattice. These two optimization problems are solved using an interior-point method and the derivative information are computed with the help of the adjoint method.

Simple numerical results demonstrate that the shape optimization problem (4.2) (without the constraints on the quality of the elements) does not always possess a solution. This result is mainly due to the fact that its feasible region is not closed. On the other hand, the shape optimization problem (4.3) (with the constraints on the quality of the elements) does non lead to the degeneracy of the physical model nor to geometrical aberrations. This shape optimization problem is then applied to an L-shaped lattice where it is shown that the proposed method **allows a significant reduction** of the strain energy. The impact of the lower bound ρ on the quality of the elements is also analyzed. Finally, the results demonstrate that a structured lattice, while geometrically simple to describe, is not necessarily an optimal lattice with respect to minimizing the strain energy.

As suggested by the last numerical results, the connectivity of the trusses affects the objective function of the optimized lattice. A forthcoming paper will investigate an adaptive procedure to gradually construct an optimized lattice from a coarse initial lattice, hence circumventing the problem of determining the connectivity of the trusses. We anticipate that the optimized lattices obtained with this adaptive method present advantageous properties compared to optimized lattice without the adaptive process.

Extension of the proposed method can be made to take into account the uncertainties in the loadings and in the manufacturing process. Also, an hierarchy of physical model with increasing complexity can be constructed within the same framework presented in Section 3 and validated. The proposed shape optimization problem (4.3) can be extended with additional design parameters such as the radius of the trusses T_m and other quality measures of the elements can be tested.

Acknowledgements

APR is grateful for the financial support of the *Fonds de recherche du Québec - Nature et technologies*. SP is grateful for the support by a Discovery Grant from the Natural Sciences and Engineering Research Council of Canada. SP also acknowledges the support by KAUST under Award Number OCRF-2014-CRG3-2281.

References

[1] W. Achtziger. On simultaneous optimization of truss geometry and topology. *Structural and Multidisciplinary Optimization*, 33(4):285–304, 2007.

[2] M. P. Bendsøe. Optimal shape design as a material distribution problem. *Structural optimization*, 1(4):193–202, 1989.

[3] M. P. Bendsøe and O. Sigmund. Material interpolation schemes in topology optimization. *Archive of Applied Mechanics*, 69(9):635–654, 1999.

[4] D. Brackett, I. Ashcroft, and R. Hague. Topology optimization for additive manufacturing. In *Proceedings of the solid freeform fabrication symposium, Austin, TX*, volume 1, pages 348–362, 2011.

[5] O. Cansizoglu, O. L. Harrysson, H. A. West II, D. R. Cormier, and T. Mahale. Applications of structural optimization in direct metal fabrication. *Rapid Prototyping Journal*, 14:114 – 122, 2008.

[6] P. Ciarlet. *The Finite Element Method for Elliptic Problems*. Society for Industrial and Applied Mathematics, 2002.

[7] B. Descamps. *Optimal shaping of lightweight structures*. PhD thesis, 2013.

[8] L. A. Freitag and P. M. Knupp. Tetrahedral element shape optimization via the jacobian determinant and condition number. In *IMR*, pages 247–258, 1999.

[9] T. Hagishita and M. Ohsaki. Topology optimization of trusses by growing ground structure method. *Structural and Multidisciplinary Optimization*, 37(4):377–393, 2009.

[10] M. Hinze, R. Pinnau, M. Ulbrich, and S. Ulbrich. *Optimization with PDE Constraints*. Springer, 2009.

[11] R. Huang, M. Riddle, D. Graziano, J. Warren, S. Das, S. Nimbalkar, J. Cresko, and E. Masanet. Energy and emissions saving potential of additive manufacturing: the case of lightweight aircraft components. *Journal of Cleaner Production*, 135:1559 – 1570, 2016.

[12] T. Munson. Mesh shape-quality optimization using the inverse mean-ratio metric. *Mathematical programming*, 110(3):561 – 590, 2007.

[13] L. E. Murr, S. M. Gaytan, F. Medina, H. Lopez, E. Martinez, B. I. Machado, D. H. Hernandez, L. Martinez, M. I. Lopez, R. B. Wicker, and J. Bracke. Next-generation biomedical implants using additive manufacturing of complex, cellular and functional mesh arrays. *Philosophical Transactions of the Royal Society of London A: Mathematical, Physical and Engineering Sciences*, 368(1917):1999–2032, 2010.

[14] J. Nocedal, A. Wachter, and R. A. Waltz. Adaptive barrier update strategies for nonlinear interior methods. *SIAM Journal on Optimization*, 19(4):1674–1693, 2009.

[15] J. Nocedal and S. J. Wright. *Numerical Optimization*. Springer, 2006.

[16] A. Öchsner and M. Merkel. *One-Dimensional Finite Elements - An Introduction to the FE Method*. Springer, 2013.

[17] P. P. Pébay and T. J. Baker. Analysis of triangle quality measures. *Mathematics of Computation*, 72(244):1817 – 1839, 2003.

[18] A. Panesar, M. Abdi, D. Hickman, and I. Ashcroft. Strategies for functionally graded lattice structures derived using topology optimisation for additive manufacturing. *Additive Manufacturing*, 19:81 – 94, 2018.

[19] A. Paquette-Rufiange. Optimisation adaptative de la topologie de lattices produits par fabrication additive. Master's thesis, 2017.

[20] G. I. N. Rozvany. A critical review of established methods of structural topology optimization. *Structural and Multidisciplinary Optimization*, 37(3):217–237, 2009.

[21] J. Smith, J. Hodgins, I. Oppenheim, and A. Witkin. Creating models of truss structures with optimization. In *Proceedings of the 29th Annual Conference on Computer Graphics and Interactive Techniques*, SIGGRAPH '02, pages 295–301, New York, NY, USA, 2002. ACM.

[22] A. Wächter. Short tutorial: Getting started with ipopt in 90 minutes. In U. Naumann, O. Schenk, H. D. Simon, and S. Toledo, editors, *Combinatorial Scientific Computing*, number 09061 in Dagstuhl Seminar Proceedings, Dagstuhl, Germany, 2009. Schloss Dagstuhl - Leibniz-Zentrum fuer Informatik, Germany.

[23] A. Wächter and L. T. Biegler. On the implementation of an interior-point filter line-search algorithm for large-scale nonlinear programming. *Mathematical Programming*, 106(1):25–57, Mar 2006.

[24] X. Wang, S. Xu, S. Zhou, W. Xu, M. Leary, P. Choong, M. Qian, M. Brandt, and Y. M. Xie. Topological design and additive manufacturing of porous metals for bone scaffolds and orthopaedic implants: A review. *Biomaterials*, 83:127 – 141, 2016.

[25] T. Zegard and G. H. Paulino. Grand — ground structure based topology optimization for arbitrary 2d domains using matlab. *Structural and Multidisciplinary Optimization*, 50(5):861–882, 2014.

[26] T. Zhao. An implementation of the ground structure method considering buckling and nodal instabilities. Master's thesis, 2014.